# Fluidized bed gas-solid heat transfer using a CFD-DEM coarse-graining technique

Document status and date:
Published: 05/10/2023

Document Version:
Publisher's PDF, also known as Version of Record (includes final page, issue and volume numbers)

Please check the document version of this publication:

• A submitted manuscript is the version of the article upon submission and before peer-review. There can be important differences between the submitted version and the official published version of record. People interested in the research are advised to contact the author for the final version of the publication, or visit the DOI to the publisher's website.
• The final author version and the galley proof are versions of the publication after peer review.
• The final published version features the final layout of the paper including the volume, issue and page numbers.

Link to publication

# Fluidized bed gas-solid heat transfer using a CFD-DEM coarse-graining technique

M.J.A. de Munck, E.A.J.F. Peters *, J.A.M. Kuipers

*Multiphase Reactors Group, Department of Chemical Engineering and Chemistry, Eindhoven University of Technology, P.O. Box 513, 5600 MB Eindhoven, the Netherlands*

## ARTICLE INFO

## ABSTRACT

Computational Fluid Dynamics - Discrete Element Method (CFD-DEM) is extensively used for modeling heat transfer in gas-solid fluidized beds. However, CFD-DEM is computationally expensive, leading to a restriction regarding the number of simulated particles. Coarse-grained CFD-DEM is a technique to circumvent this constraint, allowing one to simulate larger fluidized beds. In this work, a scaling law used for coarse-graining hydrodynamics is generalized to gas-solid heat-transfer. This approach for coarse-graining heat transfer is tested using three different superficial gas velocities where the coarse-grained particle temperatures and Nusselt numbers are obtained. The particle temperature shows good correspondence with the original system for all cases and the Nusselt number is accurately predicted by the coarse-graining scaling law.

## 1. Introduction

Drying, gas phase polymerization, granulation and biomass gasification are commonly carried out in a gas-solid fluidized bed. Fluidized beds have excellent solids mixing characteristics, leading to desired high heat and mass transfer rates. However, the gas-solid contacting pattern is very complex, leading to challenges during scale-up. Sophisticated computer models such as Computational Fluid Dynamics (CFD) - Discrete Element Method (DEM) can be applied in order to obtain a better understanding of momentum and heat transfer inside fluidized beds. The CFD-DEM (Golshan et al., 2020) technique uses an Eulerian description for the gas phase, while each particle is tracked in a Lagrangian fashion.

In the literature, the fluidized bed gas-solid contacting and heat transfer have been extensively studied using CFD-DEM (Zhou et al., 2009; Hou et al., 2012; Patil et al., 2014, 2015a,b; Wahyudi et al., 2016; Li et al., 2016, 2017; Wang et al., 2018; Mu et al., 2020a; Zhang et al., 2020; Liu et al., 2021). However, the CFD-DEM simulation scale is generally restricted due to the computationally expensive Lagrangian tracking of each individual particle. Coarse-grained CFD-DEM (Di Renzo et al., 2021) is a technique to circumvent the restriction with respect to the simulated number of particles, allowing one to simulate larger fluidized beds. Coarse-graining is based on the substitution of the actual number of DEM particles by a smaller number of larger particles while applying scaling laws. In the literature, several coarse-graining scaling laws were presented as reviewed by Di Renzo et al. (2021), see for example Sakai and Koshizuka (2009); Benyahia and Galvin (2010); Radl et al. (2011); Mu et al. (2020b).

One of the most extensively researched methods was introduced by Sakai and Koshizuka (2009) for the usage of pneumatic conveying. The scaling law was subsequently applied to fluidized beds by Sakai et al. (2010, 2014); Takabatake et al. (2018); Mori et al. (2019). In our previous work (de Munck et al., 2023), we critically analyzed the scaling law of Sakai and Koshizuka (2009) and we concluded that this method is able to well predict the gas-solid contacting in a fluidized bed. However, as stated in the review of Di Renzo et al. (2021), it becomes clear that coarse-graining scaling laws are mainly developed for describing the hydrodynamic interaction, and only a couple of researchers investigated the extension toward gas-particle heat transfer. The first contribution of coarse-graining gas-particle heat transfer was made by Lu et al. (2017). More recently, Madlmeir and Radl (2022) applied the analogy of heat and mass transfer to simulate a spray coating process. Aziz et al. (2022) modeled the fluidized bed hydrodynamics and gas-particle heat transfer by applying a coarse-graining technique. Wang and Shen (2022); Du et al. (2023) employed heat transfer coarse-graining for studying biomass gasification.

---

---

**Nomenclature**

*Roman letters*

| | | |
|---|---|---|
| $A_p$ | Particle surface area | $m^2$ |
| $C_p$ | Specific heat capacity | J/kg/K |
| $d_{p,i}$ | Particle diameter | m |
| $e_n$ | Normal restitution coefficient | - |
| $e_t$ | Tangential restitution coefficient | - |
| $\mathbf{F}_{contact,i}$ | Particle contact force | N |
| $\mathbf{g}$ | Gravitational acceleration | $m/s^2$ |
| $h$ | Heat transfer coefficient | $W/m^2/K$ |
| $\mathbf{I}$ | Unit tensor | - |
| $I_i$ | Moment of inertia | $kg \cdot m^2$ |
| $k$ | Thermal conductivity | W/m/K |
| $k_n$ | Normal stiffness | N/m |
| $k_t$ | Tangential stiffness | N/m |
| $l$ | Coarse-graining ratio | - |
| $m_i$ | Particle mass | kg |
| Nu | Nusselt number | - |
| $p_g$ | Gas pressure | Pa |
| Pr | Prandtl number | - |
| $\mathbf{q}$ | Heat flux | $W/m^2$ |
| $Q_p$ | Heat source term | $W/m^3$ |
| Re | Reynolds number | - |
| $\mathbf{S}$ | Momentum source term | $kg/m^2/s^2$ |
| $T$ | Temperature | K |
| $t$ | Time | s |
| $\mathbf{T}$ | Particle torque | $kg \cdot m/s^2$ |
| $\mathbf{u}_g$ | Gas velocity | m/s |

| | | |
|---|---|---|
| $\mathbf{r}_i$ | Particle position | m |
| $\mathbf{v}_i$ | Particle velocity | m/s |
| $V_i$ | Particle volume | $m^3$ |

*Greek letters*

| | | |
|---|---|---|
| $\beta$ | Interface momentum exchange coefficient | - |
| $\delta_n$ | Normal overlap | m |
| $\delta_t$ | Tangential overlap | m |
| $\epsilon_g$ | Gas holdup | - |
| $\eta_n$ | Normal damping coefficient | N·s/m |
| $\eta_t$ | Tangential damping coefficient | N·s/m |
| $\mu_0$ | Coefficient of friction | - |
| $\mu_g$ | Gas dynamic viscosity | kg/m/s |
| $\omega$ | Rotational velocity | 1/s |
| $\rho$ | Density | $kg/m^3$ |
| $\tau_g$ | Stress tensor | $N/m^2$ |

*Sub/superscripts*

| | |
|---|---|
| $c, j$ | Individual coarse-grained particle |
| $eff$ | Effective property |
| $g$ | Gas property |
| $i$ | Individual particle |
| $p$ | Particle property |

*Abbreviations*

| | |
|---|---|
| CFD | Computational Fluid Dynamics |
| DEM | Discrete Element Method |

In these scientific contributions, the coarse-graining extension toward gas-particle heat transfer is analyzed via the particle temperature and heat transfer rate. However, the fluidized bed gas-particle heat transfer coefficient is influenced by the gas-solid contacting pattern and the effect of coarse-graining on the interplay between the bed hydrodynamics and gas-particle heat transfer has not been extensively studied yet. The heat transfer coefficient for gas-fluidized beds is obtained via Nusselt number correlations such as the well-known Gunn (1978) correlation. This correlation is heavily dependent on the local gas holdup and particle Reynolds number. However, in coarse-graining CFD-DEM simulations, numerical errors in the solids holdup potentially arise due to the increased particle-size relative to the grid-cell size used to solve the gas phase conservation equations. Applying a smoothing function with a length scale independent of the grid size for interpolating and distributing between Lagrangian and Eulerian quantities (see Deen et al. (2004); de Munck et al. (2023)) is therefore expected to be a key factor for accurate coarse-grained gas-particle heat transfer.

In this work, the CFD-DEM model used by de Munck et al. (2023) is extended for gas-particle heat transfer. The CFD-DEM model combines the CFD framework FoxBerry (Kamath et al., 2020) with the DEM code MercuryDPM (Weinhart et al., 2020). This paper is organized as follows. The coarse-graining CFD-DEM modeling methods, including gas-particle heat transfer, are described in the next section. Thereafter, we verify the two-way gas-particle heat transfer coupling by making use of an analytical solution. The simulation setup for the fluidized bed study is given in Section 4. We present the coarse-graining fluidized bed results in Section 5 where we critically analyze the coarse-graining scaling law via the particle temperature and Nusselt number. A final conclusion on the suitability of the gas-particle heat transfer scaling law is given in Section 6.

## 2. Modeling method

### 2.1. General equations

The gas phase is described by the continuity equation and the volume-averaged Navier-Stokes equations, respectively given by:

$$\frac{\partial(\epsilon_g \rho_g)}{\partial t} + \nabla \cdot (\epsilon_g \rho_g \mathbf{u}_g) = 0 \tag{1}$$

$$\frac{\partial (\epsilon_g \rho_g \mathbf{u}_g)}{\partial t} + \nabla \cdot (\epsilon_g \rho_g \mathbf{u}_g \mathbf{u}_g) = -\epsilon_g \nabla p_g - \nabla \cdot (\epsilon_g \tau_g) - \mathbf{S} + \epsilon_g \rho_g \mathbf{g} \tag{2}$$

where the gas phase density is calculated according to the ideal gas law shown by:

$$\rho_g = \frac{p_g M}{R T_g} \tag{3}$$

$\tau_g$ is the gas phase stress tensor using the general Newtonian form. $\mathbf{S}$ represents the momentum source term for the gas-solids interaction, given by:

$$\mathbf{S} = \sum_i 3\pi \mu_g \epsilon_g d_{p,i} \beta (\mathbf{u}_g - \mathbf{v}_i) D (\mathbf{r} - \mathbf{r}_i) \tag{4}$$

The momentum source term contribution is implemented via a semi-implicit method (Kuipers et al., 1993; Verma et al., 2013; Patil et al., 2014; de Munck et al., 2023). In equation (4), $D$ stands for the polynomial distribution function of Deen et al. (2004) using the particle position $\mathbf{r}_i$ relative to the computational cell $\mathbf{r}$. A mapping width of $3d_p$ is applied. For more detailed information about the Euler–Lagrange coupling method, see Deen et al. (2004) and Lau et al. (2014). The interface momentum exchange coefficient, $\beta$, describes the drag of the gas phase acting on a particle, which is calculated via a drag force closure. In this work, the drag correlation proposed by (Beetstra et al., 2007) is used:

$$\beta = 10\frac{(1-\epsilon_g)}{\epsilon_g^2} + \epsilon_g^2\left(1 + 1.5\sqrt{1-\epsilon_g}\right)$$
$$+ \frac{0.413 Re_p}{24\epsilon_g^2}\frac{\left[\epsilon_g^{-1} + 3\epsilon_g(1-\epsilon_g) + 8.4 Re_p^{-0.343}\right]}{\left[1 + 10^{3(1-\epsilon_g)} Re_p^{-0.5-2(1-\epsilon_g)}\right]} \quad (5)$$

with

$$Re_p = \frac{\epsilon_g \rho_g \left|\mathbf{u}_g - \mathbf{v}_p\right| d_p}{\mu_g} \quad (6)$$

The gas phase thermal energy balance is represented by equation (7),

$$C_{p,g}\left[\frac{\partial\left(\epsilon_g \rho_g T_g\right)}{\partial t} + \nabla\cdot\left(\epsilon_g \rho_g \mathbf{u}_g T_g\right)\right] = -\nabla\cdot\left(\epsilon_g \mathbf{q}\right) + Q_p \quad (7)$$

where $Q_p$ represents the source term originating from the interphase heat exchange with the particles as given by equation (8). The heat source term contribution is represented by equation (8) and is treated in a linear-implicit fashion.

$$Q_p = \sum_i h_{p,i} A_{p,i}(T_{p,i} - T_g)D\left(\mathbf{r} - \mathbf{r}_i\right) \quad (8)$$

The gas-particle heat transfer coefficient ($h_{p,i}$), is calculated using the empirical Gunn correlation (Gunn, 1978) given by:

$$Nu_p = (7 - 10\epsilon_g + 5\epsilon_g^2)(1 + 0.7 Re_p^{0.2} Pr^{1/3})$$
$$+ (1.33 - 2.40\epsilon_g + 1.20\epsilon_g^2)Re_p^{0.7} Pr^{1/3} \quad (9)$$

using:

$$Nu_p = \frac{h_p d_p}{k_g}; \qquad Pr = \frac{\mu_g C_{p,g}}{k_g} \quad (10)$$

The heat conduction is given by Fourier's law using an effective conductivity (Syamlal and Gidaspow, 1985):

$$\mathbf{q} = -k_g^{eff}\nabla T_g \quad (11)$$

$$k_g^{eff} = \frac{1 - \sqrt{1-\epsilon_g}}{\epsilon_g}k_g \quad (12)$$

The translational and rotational movement of each individual particle can be obtained by solving Newton's equations, respectively given by equation (13) and (14):

$$m_i\frac{d\mathbf{v}_i}{dt} = -V_i\nabla p_g + 3\pi\mu_g\epsilon_g d_{p,i}\beta\left(\mathbf{u}_g - \mathbf{v}_i\right) + m_i\mathbf{g} + \sum\mathbf{F}_{contact,i} \quad (13)$$

$$I_i\frac{\omega_i}{dt} = \mathbf{T}_i \quad (14)$$

where $\mathbf{v}_i$ is the particle velocity. The forces on the right-hand side for the translational motion (equation (13)) are respectively due to the far-field pressure gradient, drag, gravity and contact forces due to particle-particle or particle-wall collisions. The contact forces are captured by a soft-sphere model originally developed by Cundall and Strack (1979). $\mathbf{T}_i$ is the torque, $I_i$ the moment of inertia and $\omega_i$ the rotational velocity. The thermal energy equation for each individual particle is given by:

$$\rho_{p,i}C_{p,i}V_{p,i}\frac{dT_{p,i}}{dt} = -h_{p,i}A_{p,i}(T_{p,i} - T_g) \quad (15)$$

where $h_{p,i}$ is the earlier mentioned heat transfer coefficient obtained via the Nusselt number, see equation (10).

## 2.2. Scaling model

In the scaling model of Sakai and Koshizuka (2009) the total particle mass and volume of the coarse-grained system is equal to the original system (coarse-graining ratio equal to 1). A coarse-grained particle represents $l^3$ original particles, where $l$ stands for the coarse-graining ratio. The particle diameter is scaled with a factor $l$. Hence, the number of

particles in a coarse-grained system will reduce with a factor $l^{-3}$. As discussed by de Munck et al. (2023) the Beetstra drag model should be scaled using an additional factor $l^2$ in order to scale the drag force with a factor $l^3$, thus $\beta_c = l^2\beta$. Applying a coarse-graining ratio equal to 1 shows that the original balance, given in equation (13), is obtained. The scaling with $l$ is such that the kinematics of the coarse-grained particle is similar to that of the original (non-coarse grained) particle. This means that both the velocity and the acceleration remain the same irrespective of $l$. Since $m_{c,j}$ scales with $l^3$ all forces on the right-hand side should scale with $l^3$ as well.

$$m_{c,j}\frac{d\mathbf{v}_{c,j}}{dt} = -V_{c,j}\nabla p_g + 3\pi\mu_g\epsilon_g d_{p,c,j}\beta_c\left(\mathbf{u}_g - \mathbf{v}_{c,j}\right) + m_{c,j}\mathbf{g} + \sum\mathbf{F}_{contact_{c,j}} \quad (16)$$

The Reynolds number used inside the Beetstra drag correlation is unchanged by using the original particle diameter:

$$Re_c = \frac{\epsilon_g \rho_g \left|\mathbf{u}_g - \mathbf{v}_c\right| d_p}{\mu_g} \quad (17)$$

The contact force contribution in equation (16) uses the linear spring-dashpot model, where the normal component is scaled with a factor $l^3$ using $k_{n,c} = l^3 k_n$ and $\eta_{n,c} = l^3\eta_n$. $k_n$, $\delta_n$ and $\eta_n$ are respectively the normal stiffness, the overlap and the damping coefficient.

$$\mathbf{F}_{contact,n_{c,j}} = \left(-k_{n,c}\delta_{n_{c,j}} - \eta_{n,c}\mathbf{v}_{n_{c,j}}\right) \quad (18)$$

In a similar fashion, the tangential component of the contact force is given by:

$$\mathbf{F}_{contact,t_{c,j}} = \begin{cases} \left(-k_{t,c}\delta_{t_{c,j}} - \eta_{t,c}\mathbf{v}_{t_{c,j}}\right) & \text{if } |\mathbf{F}_{contact,t_{c,j}}| \leq \mu_0|\mathbf{F}_{contact,n_{c,j}}| \\ -\mu_0|\mathbf{F}_{contact,n_{c,j}}|\frac{\mathbf{v}_{t_{c,j}}}{|\mathbf{v}_{t_{c,j}}|} & \text{if } |\mathbf{F}_{contact,t_{c,j}}| > \mu_0|\mathbf{F}_{contact,n_{c,j}}| \end{cases} \quad (19)$$

where $\mu_0$ is the friction coefficient, $k_{t,c}$ the coarse-graining tangential stiffness (using $k_{t,c} = l^3 k_t$), $\delta_t$ the overlap and $\eta_{t,c}$ the coarse-graining damping coefficient (using $\eta_{t,c} = l^3\eta_t$). Using the rotational motion shown in equation (14), the coarse-grained rotational motion becomes:

$$\frac{d\omega_{c,j}}{dt} = \frac{\mathbf{T}_{c,j}}{I_{c,j}} = \frac{l^4 \mathbf{T}_i}{l^5 I_i} = \frac{1}{l}\frac{d\omega_i}{dt} \quad (20)$$

This scaling is such that the surface velocity of the particle remains the same independent of $l$. This is also important for the ratio between normal and tangential contact forces.

## Heat transfer

The Nusselt correlation for coarse-graining systems uses the Reynolds number based on the original particle diameter (see equation (17)). The Prandtl number is independent of the level of coarse-graining since the gas phase properties remain constant. Furthermore, the Gunn correlation (shown in equation (9)) is heavily dependent on the local gas holdup. As shown by de Munck et al. (2023), unaffected two-way coupling upon coarse-graining leads to unchanged porosity values compared to the base case. The coarse-grained heat transfer coefficient becomes:

$$h_c = Nu_c(Re_c, Pr)\frac{k_g}{d_{p,c}}l^2 \quad (21)$$

Besides, the particle volume (scaled by $l^3$) and area (scaled by $l^2$) in the particle thermal energy balance are scaled according to the previously mentioned scaling rules. Therefore, both sides of the coarse-grained particle thermal energy balance, shown in equation (22), are scaled by $l^3$ due to $V_{c,j} = l^3 V_{p,i}$ and $h_{c,j}A_{c,j} = l^3 h_{p,i}A_{p,i}$. Please note, the particle density and specific heat capacity remain constant upon coarse-graining.

**Table 1**
Simulation settings used for the fixed bed verification test. The bold values indicate that proper scaling needs to be applied.

| Parameter | Symbol | Value | Unit |
|---|---|---|---|
| Particle diameter | $d_p$ | **$4.875 \cdot 10^{-4}$** | m |
| Inlet velocity | $u_0$ | 0.1 | m/s |
| Fluid density | $\rho_g$ | 300 | kg/m³ |
| Fluid heat capacity | $C_{p,g}$ | 1000 | J/kg/K |
| Fluid thermal conductivity | $k_g$ | 0.025 | W/m/K |
| Particle density | $\rho_p$ | 800 | kg/m³ |
| Particle heat capacity | $C_{p,p}$ | 1500 | J/kg/K |
| Number of grid cells (width) | Nx | 10 | - |
| Number of grid cells (depth) | Ny | 10 | - |
| Number of grid cells (height) | Nz | 400 | - |

$$\rho_{c,j} C_{c,j} V_{c,j} \frac{dT_{c,j}}{dt} = -h_{c,j} A_{c,j}(T_{c,j} - T_g) \tag{22}$$

## 3. Verification

A fixed bed test is performed in order to verify the two-way heat transfer coupling. A column with dimensions $0.6 \times 0.015 \times 0.015$ m (height × width × depth) was utilized. In this test, a bed of initially cold particles and cold fluid (at 293 K) was heated by injecting a hot fluid (393 K) from the bottom with a superficial velocity equal to 0.1 m/s. During this transient simulation, both the fluid and particles will heat up, resulting in a heat front propagating in the axial direction. The simulation parameters are summarized in Table 1. Please note, the grid cell size is constant upon coarse-graining.

The simulation results can be verified with a one-dimensional analytical convection equation which takes into account the interphase heat transfer between the fluid and particle phase. The thermal conduction can be neglected due to the very high Péclet number (Pe ≫ 100). The one-dimensional energy balances for the fluid and particle phase are given by:

$$\epsilon_g \rho_g C_{p,g} \frac{\partial T_{g,z}}{\partial t} = -\epsilon_g \rho_g C_{p,g} u_z \frac{\partial T_{g,z}}{\partial z} - ha(T_{g,z} - T_{p,z}) \tag{23}$$

$$(1 - \epsilon_g) \rho_p C_{p,p} \frac{\partial T_{p,z}}{\partial t} = ha(T_{g,z} - T_{p,z}) \tag{24}$$

where $a$ is the specific interfacial area given by:

$$a = 6 \frac{(1 - \epsilon_g)}{d_p} \tag{25}$$

Details of the analytical solution for the set of equations can be found in Bird et al. (2007) and Patil et al. (2014). In coarse-graining fluidized bed simulations, it is known that the gas-particle heat transfer is dependent on the bed hydrodynamics. In order to judge the capabilities of the coarse-grained gas-particle heat transfer scaling law given in the previous section, the fixed bed test is also carried out for coarse-grained systems up to 2.5 times the original system and therefore, this verification serves two purposes. Fig. 1 presents the comparison between the analytical solution and the simulation results for different simulation times. It can be concluded from this test that the gas-particle heat transfer is well implemented for the original system. Besides, applying the scaling law for two-way gas-particle heat transfer results in perfect coincidence with the analytical solution.

## 4. Simulation setup

In the next step, the gas-particle heat transfer was simulated in a 3D gas-fluidized bed with dimensions $0.2 \times 0.04 \times 0.025$ m (height × width × depth). Three different superficial gas velocities equal to 0.14, 0.2 and 0.3 m/s were examined. In the base case, 720 000 $\gamma$-$A_2O_3$ particles were used whereof the DEM collision properties were obtained from Sutkar et al. (2013). The scaling law was studied using
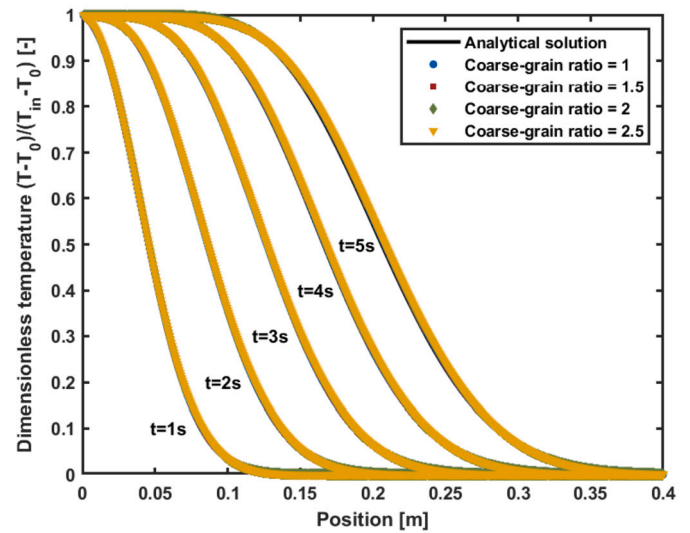


**Fig. 1.** Dimensionless temperature profiles of a fixed bed heat transfer case compared with an analytical solution.

**Table 2**
Parameters used for investigating the coarse-graining gas-particle heat transfer coupling in a 3D fluidized bed. The bold values indicate that proper scaling needs to be applied.

| Parameter | Symbol | Value | Unit |
|---|---|---|---|
| Particle diameter | $d_p$ | **$5 \cdot 10^{-4}$** | m |
| Inlet velocity air | $u_0$ | 0.14, 0.20 and 0.30 | m/s |
| Particle density | $\rho_p$ | 1040 | kg/m³ |
| Particle heat capacity | $C_p$ | 779 | J/kg/K |
| Friction coefficient | $\mu_0$ | 0.1 | - |
| Normal coefficient of restitution | $e_n$ | 0.74 | - |
| Tangential coefficient of restitution | $e_t$ | 0.1 | - |
| Normal stiffness | $k_n$ | **500** | N/m |
| Tangential stiffness | $k_t$ | **217.60** | N/m |
| Normal dampening coefficient | $\eta_n$ | **$7.9 \cdot 10^{-4}$** | N·s/m |
| Tangential dampening coefficient | $\eta_t$ | **$1.7 \cdot 10^{-3}$** | N·s/m |
| CFD time step | $t_{flow}$ | $2.5 \cdot 10^{-5}$ | s |
| DEM time step | $t_{DEM}$ | $2.5 \cdot 10^{-6}$ | s |
| Time simulated | $t$ | 25 | s |
| Number of grid cells (width) | Nx | 32 | - |
| Number of grid cells (depth) | Ny | 20 | - |
| Number of grid cells (height) | Nz | 160 | - |

coarse-graining ratios 1.5, 2, 2.5. The resulting numbers of particles were equal to 213 333, 90 000 and 46 080 respectively. The maximum studied coarse-graining ratio is relatively low due to the chosen domain size. A larger domain automatically results in an unfeasible number of particles for the non-coarse-grained system. The simulation parameters are listed in Table 2. See Deen et al. (2007) for more details about calculating the spring stiffness and damping coefficient. Please note, the grid cell size is constant upon coarse-graining. In the initialization step, hot $\gamma$-$A_2O_3$ particles (363.15 K) were placed in a lattice structure. Cold nitrogen gas (293.15 K) was injected from the bottom using a uniform superficial velocity boundary condition equal to 0.14, 0.2 and 0.3 m/s. During this process, the hot solid material will cool down due to the heat exchange with the cold gas. Furthermore, a no-slip boundary condition for the side walls and a fixed pressure boundary condition of 1 atm at the top of the domain were applied. A homogeneous Neumann boundary condition for the side walls was applied for solving the gas phase thermal energy balance implying that no heat is lost through these walls.
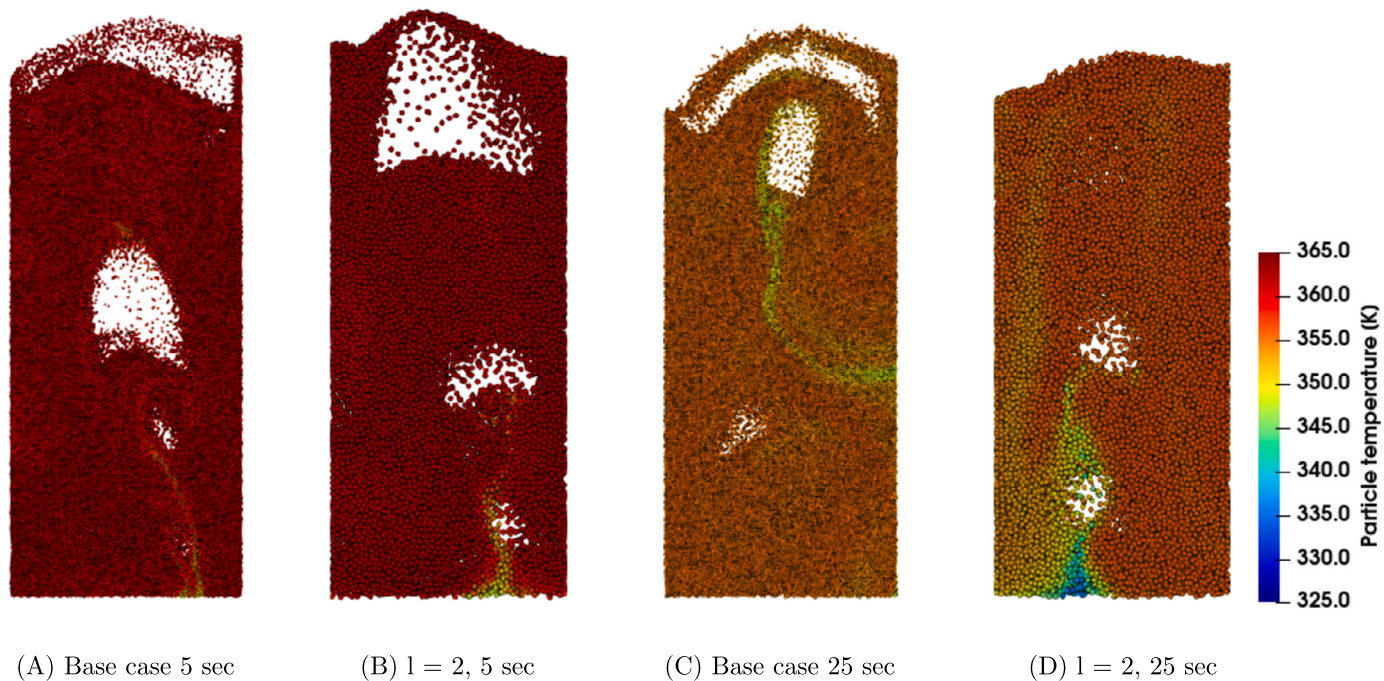
(A) Base case 5 sec          (B) l = 2, 5 sec          (C) Base case 25 sec          (D) l = 2, 25 sec

**Fig. 2.** Instantaneous particle configurations near the center plane of the column for the base case (A, C) and coarse-graining ratio, l, equal to 2 (B, D) taken at 5 and 25 seconds. The superficial velocity is equal to 0.14 m/s. Due to the cold injected gas, the solids temperature decreases.
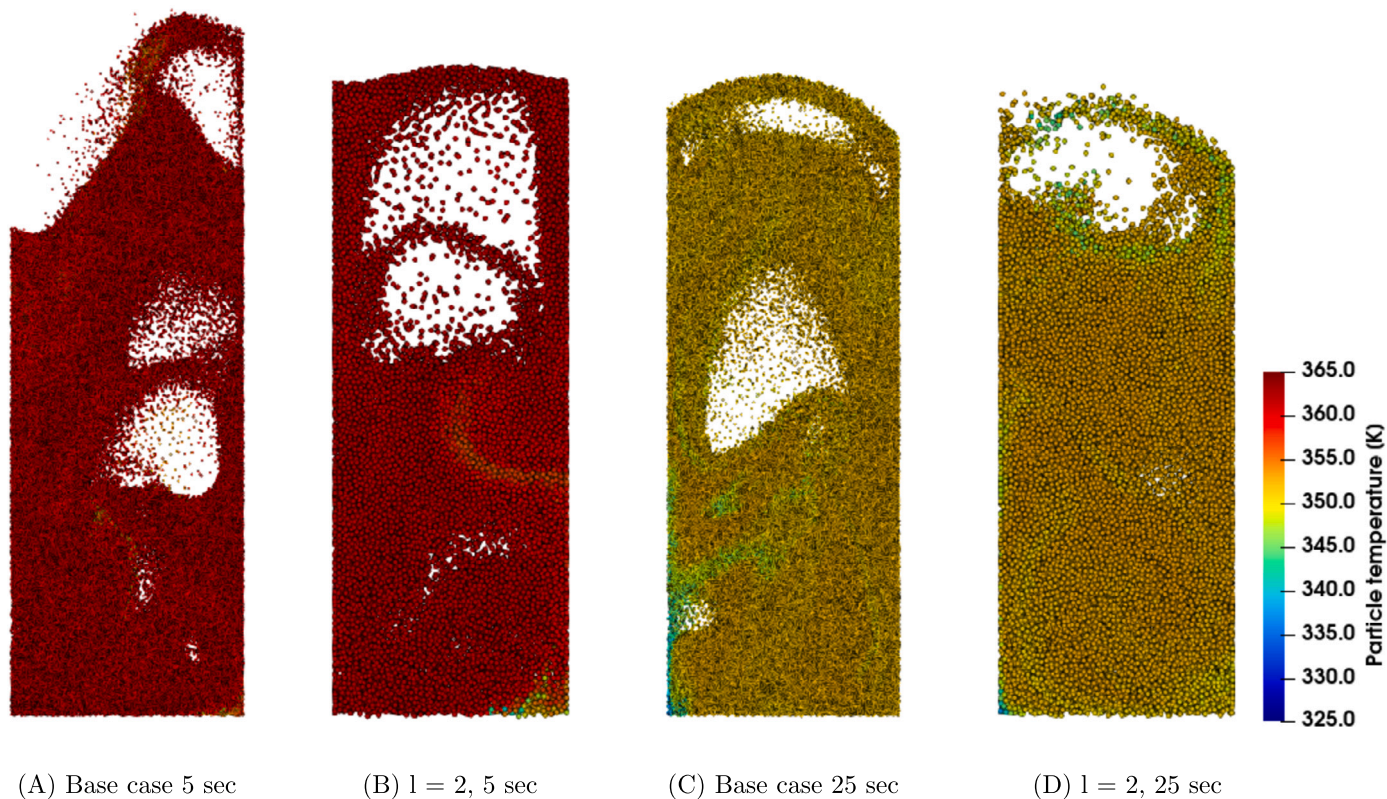


(A) Base case 5 sec          (B) l = 2, 5 sec          (C) Base case 25 sec          (D) l = 2, 25 sec

**Fig. 3.** Instantaneous particle configurations near the center plane of the column for the base case (A, C) and coarse-graining ratio, l, equal to 2 (B, D) taken at 5 and 25 seconds. The superficial velocity is equal to 0.20 m/s. Due to the cold injected gas, the solids temperature decreases.
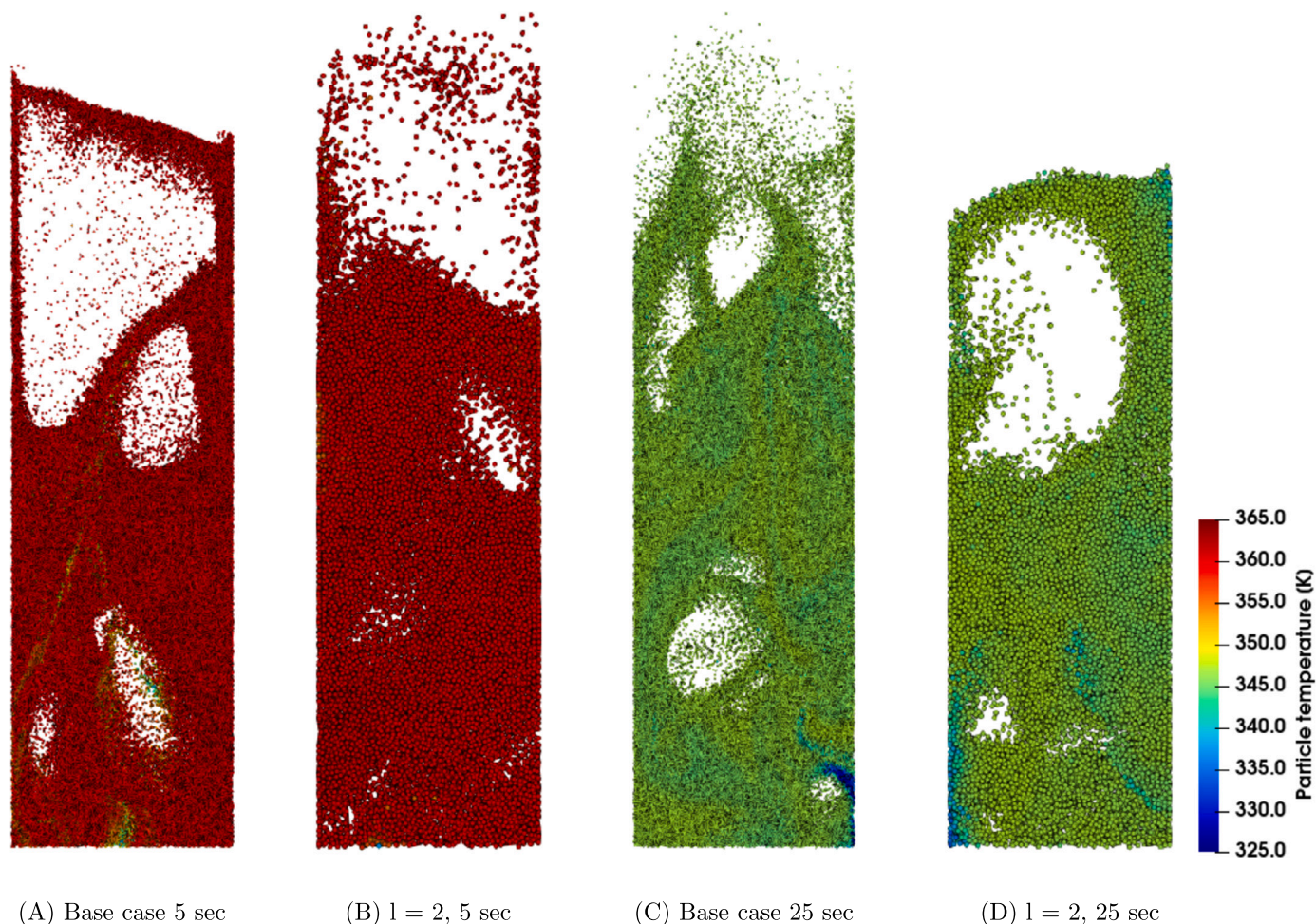
(A) Base case 5 sec      (B) l = 2, 5 sec      (C) Base case 25 sec      (D) l = 2, 25 sec

**Fig. 4.** Instantaneous particle configurations near the center plane of the column for the base case (A, C) and coarse-graining ratio, l, equal to 2 (B, D) taken at 5 and 25 seconds. The superficial velocity is equal to 0.30 m/s. Due to the cold injected gas, the solids temperature decreases.

## 5. Results and discussion

### 5.1. Particle configurations

In this paragraph, the particle temperature upon coarse-graining is analyzed for the three different applied superficial gas velocities. Figs. 2, 3 and 4 present instantaneous particle configurations near the center plane of the column for the 0.14, 0.20 and 0.30 m/s superficial velocity cases, respectively. The instantaneous particle configurations are taken at 5 and 25 seconds for the base case (i.e. no applied scaling) and for the case of scaling ratio equal to 2. Initially, the particles have a temperature equal to 363.15 K. Due to the cold injected gas (293.15 K), the solids temperature decreases. Please note, identical temperature color bars between Figs. 2, 3 and 4 were applied in order to show the larger particle temperature decrease when a larger volumetric gas flow rate is applied. When the superficial gas velocity is increased, the size of the bubbles also increases. This happens because the higher velocity leads to enhanced bubble coalescence. This effect is clearly observed by comparing the three different superficial velocity cases. It is also seen that the larger bubbles result in a larger bed expansion.

The coarse-graining scaling law is able to well describe both the bed hydrodynamics and particle temperature. The bed hydrodynamics were examined in previous works, see Sakai et al. (2010, 2014); de Munck et al. (2023). Similar to the base case systems, the coarse-grained simulations also display more chaotic bed movement when the superficial gas velocity is increased. Besides, the increased bed expansion is clearly visible in the snapshots. Furthermore, it is seen that the particle tem-perature for coarse-grained systems is similar to the base case systems. However, it is hard to draw quantitative conclusions from the individual snapshots and consequently, a more in-depth analysis is needed.

### 5.2. Particle temperature

Fig. 5 shows the mean particle temperature versus time. Initially, the particle temperature was set to 363.15 K and due to the cold injected gas (293.15 K), the solids temperature decreases. The gas volumetric flow rate increases upon increasing the superficial gas velocity. Therefore a faster temperature decline is obtained for higher superficial gas velocities. It can be observed that the coarse-graining scaling law is able to predict the mean particle temperature over time with very high accuracy.

The instantaneous normalized particle temperature probability density function (PDF) is able to give more detailed information about the decreasing particle temperatures over time. Fig. 6 shows the instantaneous PDF for the three studied superficial velocities at 5, 15 and 25 seconds. The instantaneous PDFs have a pronounced tail towards the colder temperatures for all simulations, whereof the size decreases upon increasing the superficial gas velocity. This can be explained by the solids mixing rate in the bed. At low superficial gas velocities, the solids mixing and circulation are less intense. Therefore, solids located in the bottom region experience larger contact times with cold gas, resulting in relatively cold solids. These findings are in correspondence with the observations of Li et al. (2016).
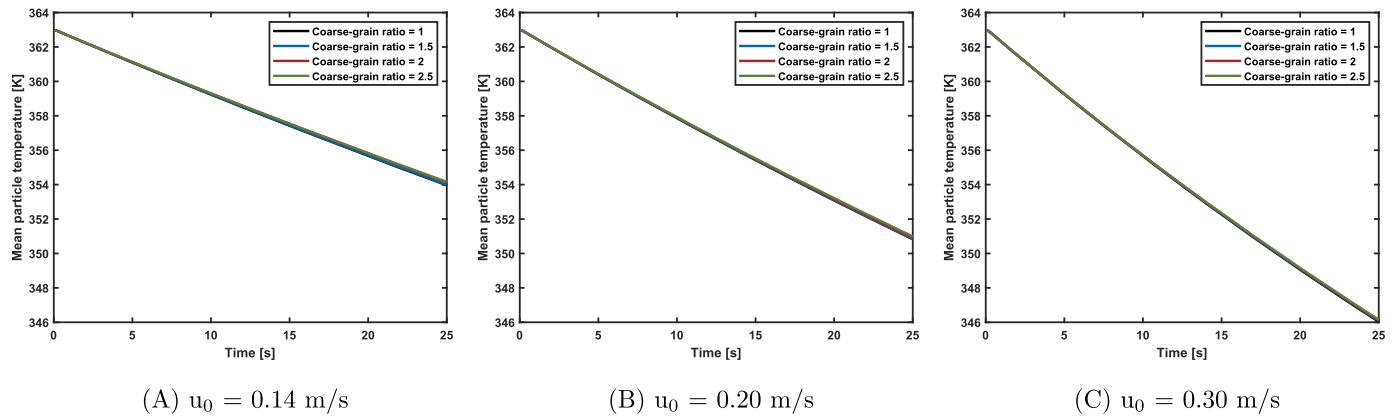
(A) $u_0 = 0.14$ m/s

(B) $u_0 = 0.20$ m/s

(C) $u_0 = 0.30$ m/s

**Fig. 5.** Mean particle temperature versus time for three superficial velocities ($u_0$ = 0.14, 0.20 and 0.30 m/s). Due to the cold injected gas, the solids temperature decreases. The coarse-graining scaling law is able to perfectly predict the original mean particle temperature.
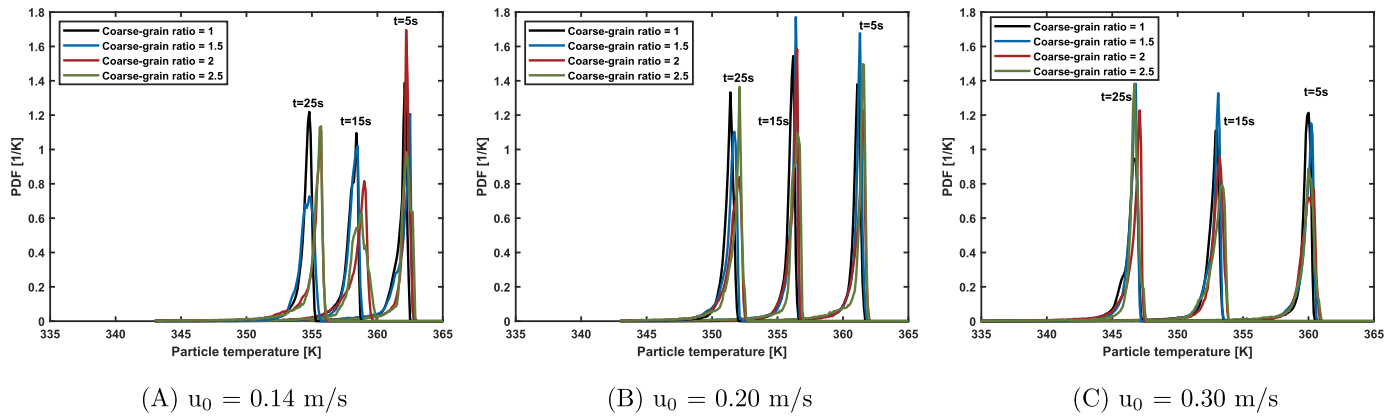


(A) $u_0 = 0.14$ m/s

(B) $u_0 = 0.20$ m/s

(C) $u_0 = 0.30$ m/s

**Fig. 6.** Instantaneous particle temperature PDF for 5, 15 and 25 seconds for the three studied superficial velocities ($u_0$ = 0.14, 0.20 and 0.30 m/s). Due to the cold injected gas, the solids temperature decreases. The coarse-graining scaling law shows good correspondence with the original system.
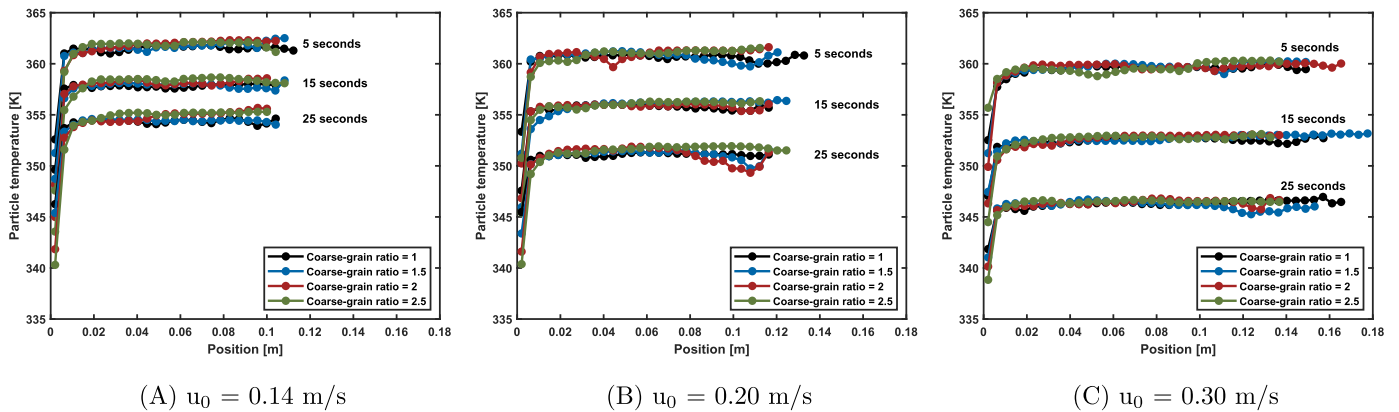


(A) $u_0 = 0.14$ m/s

(B) $u_0 = 0.20$ m/s

(C) $u_0 = 0.30$ m/s

**Fig. 7.** Particle temperature over the axial position for the three studied superficial velocities ($u_0$ = 0.14, 0.20 and 0.30 m/s). The coarse-graining scaling law shows good correspondence with the original system.

Similar to the particle mean temperature, the coarse-graining scaling law describes the temperature decline accurately. However, it should be noted that subtle differences between the probability density functions are found. This can be explained by the following. The cold injected gas cools down the hot solid bed material and the gas-particle temperature driving force quickly decreases. Therefore, all thermal energy available to cool down the bed is transferred to the solid material before the gas reaches the freeboard region, resulting in an accurate description of the average particle temperature. However, upon coarse-graining, a difference in the local energy transfer inside the bed is found, which

is displayed by the small discrepancies in the instantaneous PDFs. This difference is reduced by increasing the superficial gas velocity.

The local temperature differences are further analyzed by the axial temperature profiles, shown in Fig. 7. Similar to the average particle temperature, a larger temperature decrease is noted over time upon increasing the superficial gas velocity. Besides, more bed expansion is observed. However, it should be noted that the length of the shown instantaneous axial temperature profiles could differ since bubble formation, propagation and eruption is a very dynamic process. As stated in the previous paragraph, increasing the superficial gas velocity results
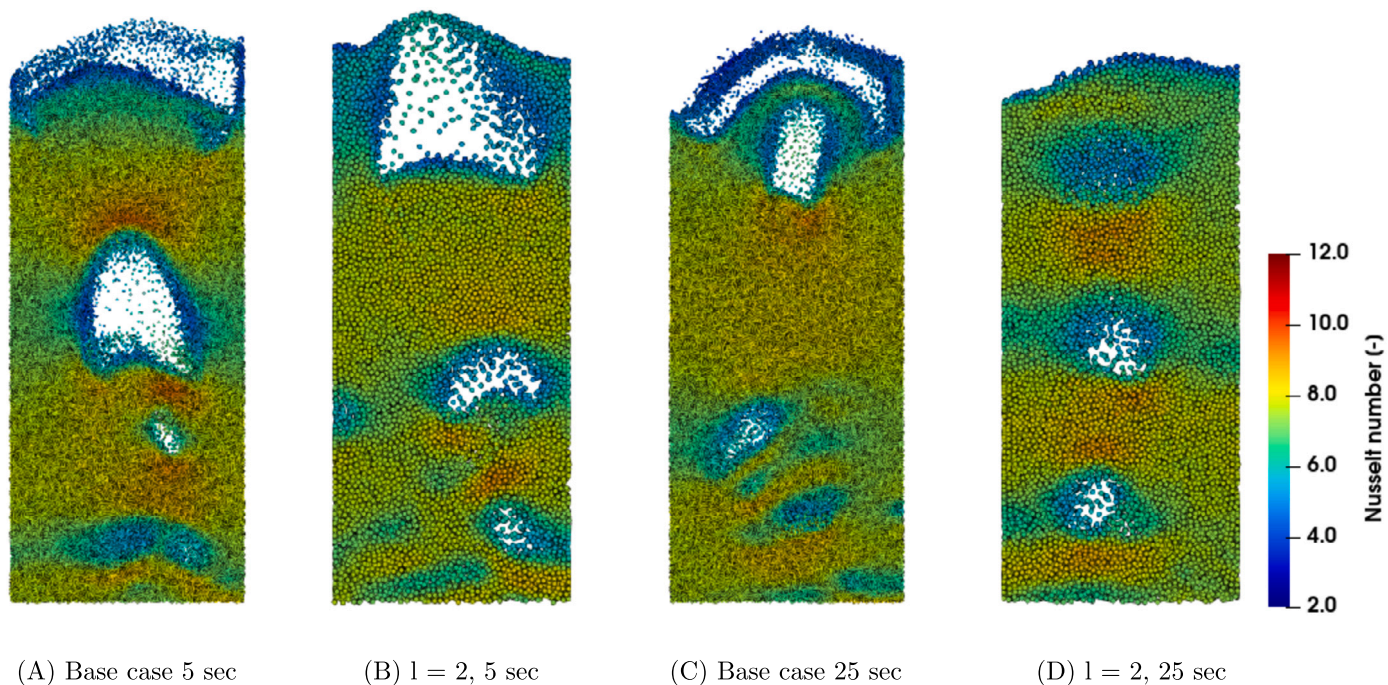
(A) Base case 5 sec          (B) l = 2, 5 sec          (C) Base case 25 sec          (D) l = 2, 25 sec

**Fig. 8.** Instantaneous particle configurations near the center plane of the column for the base case (A, C) and coarse-graining ratio, l, equal to 2 (B, D) taken at 5 and 25 seconds. The superficial velocity is equal to 0.14 m/s. The instantaneous Nusselt number is well described by the coarse-graining scaling law.
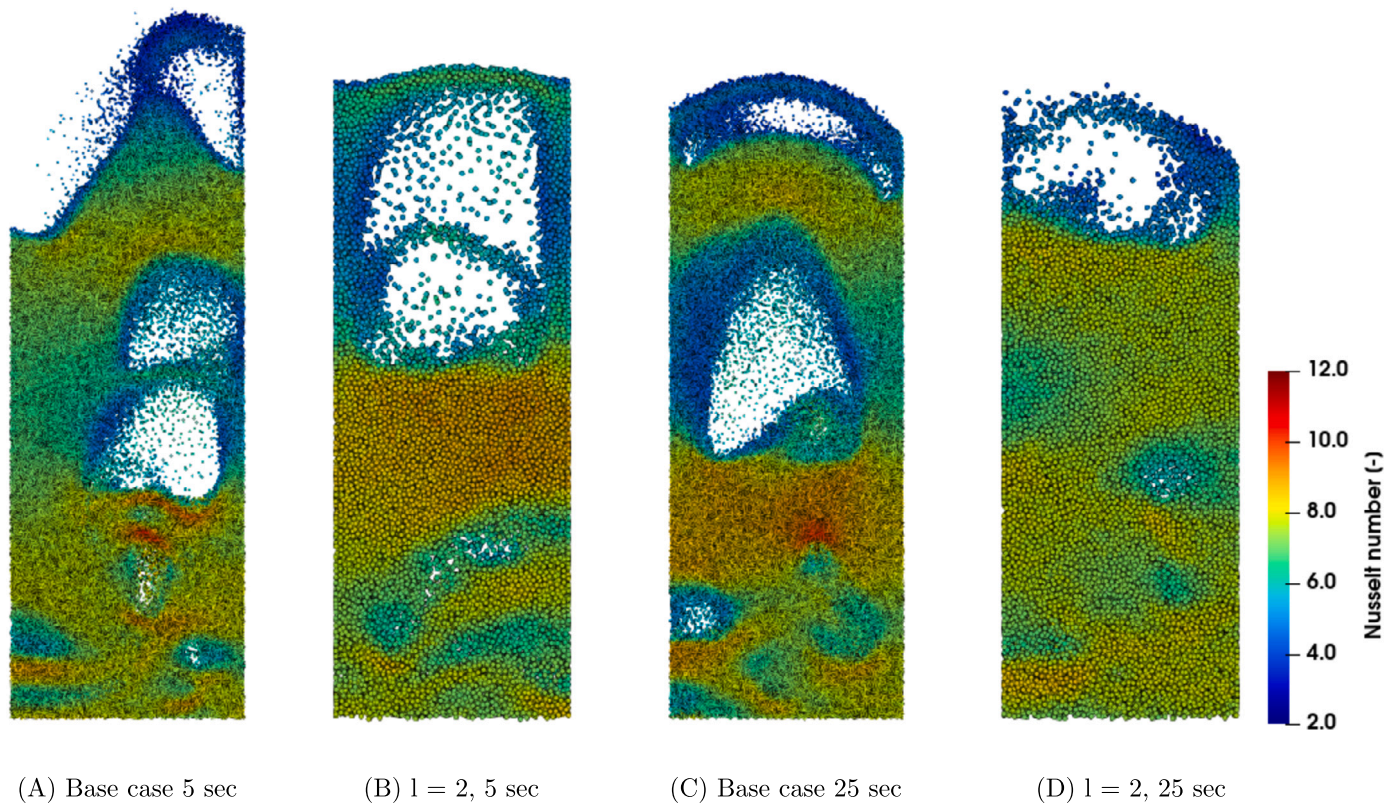


(A) Base case 5 sec          (B) l = 2, 5 sec          (C) Base case 25 sec          (D) l = 2, 25 sec

**Fig. 9.** Instantaneous particle configurations near the center plane of the column for the base case (A, C) and coarse-graining ratio, l, equal to 2 (B, D) taken at 5 and 25 seconds. The superficial velocity is equal to 0.20 m/s. The instantaneous Nusselt number is well described by the coarse-graining scaling law.
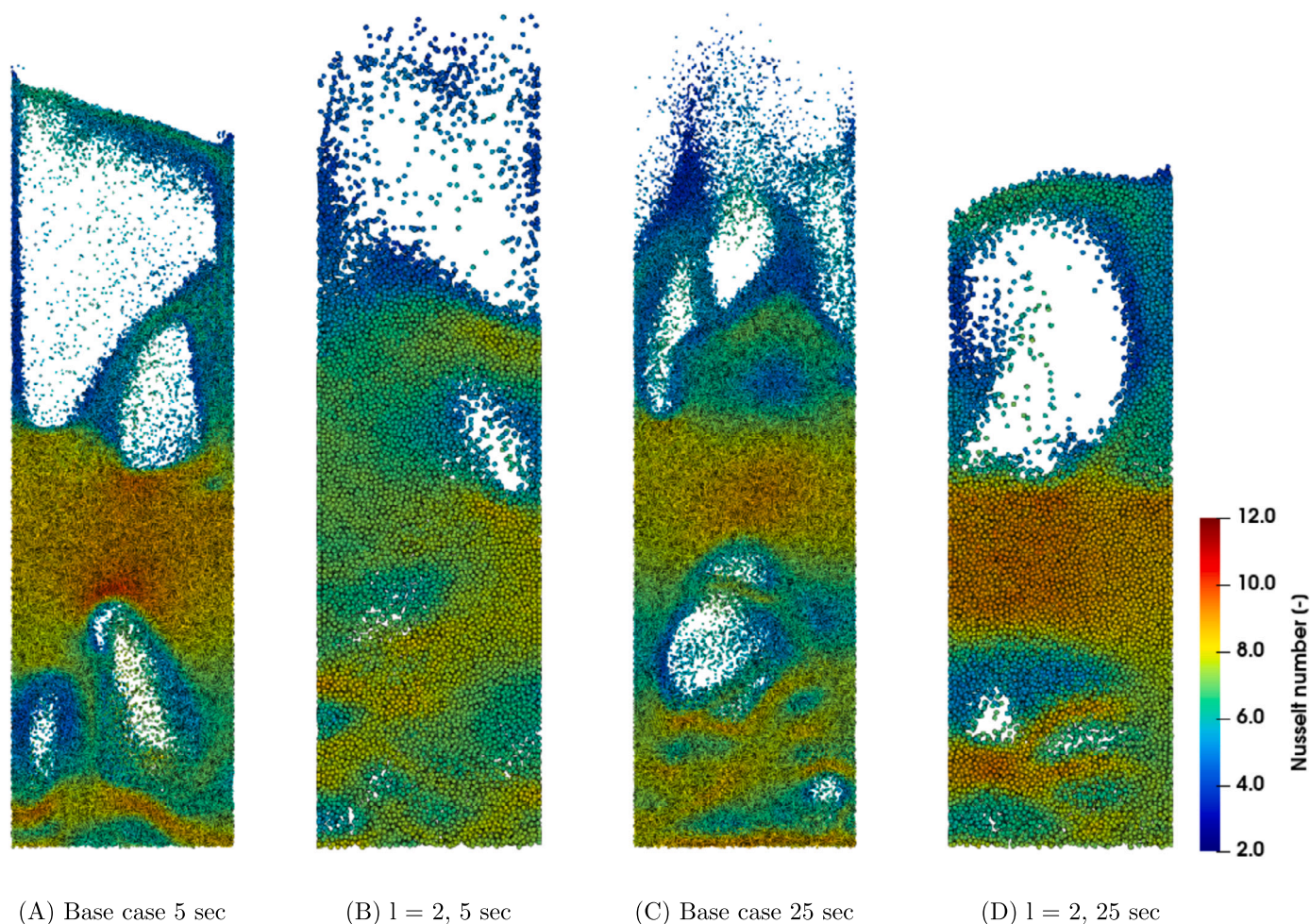
(A) Base case 5 sec      (B) l = 2, 5 sec      (C) Base case 25 sec      (D) l = 2, 25 sec

**Fig. 10.** Instantaneous particle configurations near the center plane of the column for the base case (A, C) and coarse-graining ratio, l, equal to 2 (B, D) taken at 5 and 25 seconds. The superficial velocity is equal to 0.30 m/s. The instantaneous Nusselt number is well described by the coarse-graining scaling law.

in more vigorous bed mixing and a higher solids circulation rate, leading to smaller cold temperature tails. The bottom (cold) temperature region in the case of a low superficial gas velocity is less accurately described due to the averaging nature of coarse-graining. In the coarse-graining simulations, the bottom-located particles are relatively colder, whereas the particles located up in the bed have a higher temperature.

*5.3. Gas-particle Nusselt number*

In the previous subsection, the particle temperature was discussed. However, due to the good mixing properties of the fluidized bed, almost all heat is transferred from the inlet gas to the bed. One might object that, if there are significant differences in heat transfer rates upon coarse-graining, these differences remain largely unnoticed if we look solely at the temperature. Therefore, we here report also directly on the heat transfer rates. The gas-particle heat transfer coefficient is obtained using the Gunn correlation (see equation (9)). The Gunn correlation is heavily dependent on the local gas holdup and it should be noted that with an increasing local gas holdup, the Nusselt number decreases.

Figs. 8, 9 and 10 present instantaneous particle configurations and the corresponding Nusselt numbers near the center plane of the column for the 0.14, 0.20 and 0.30 m/s superficial velocity cases respectively. The instantaneous particle configurations are taken at 5 and 25 seconds and present the simulation results for the base case (i.e. no applied scaling) and scaling ratio equal to 2. As discussed in the previous subsection, an increase in the superficial gas velocity results in larger

bubbles, caused by the increased rate of bubble coalescence. This has a clear effect on the local Nusselt number. Upon increasing the superficial gas velocity, larger local differences in the Nusselt number are obtained. Similar to Li et al. (2016), the highest Nusselt number values are found in the bubble wake, while in the bubble clouds, relatively low values are found. It is observed that the coarse-graining scaling law predicts this behavior quite accurately. However, a coarse-graining representation simulates *N* number of original particles. This means that coarse-graining averages the behavior of the original system and this leads to less pronounced bubble wake and cloud regions. Since both the bubble wake and cloud regions result in typically the highest and lowest Nusselt numbers respectively, it is expected that coarse-graining does not fully capture the effects present in these regions.

The time and spatially averaged Nusselt number upon coarse-graining for the three different superficial gas velocities is shown in Fig. 11. The first 2.5 seconds are discarded in this analysis in order to avoid startup effects. Similar to Li et al. (2016); Banaei et al. (2017) we found that the average Nusselt number is decreasing at higher superficial gas velocities. Li et al. (2016) found that upon fluidization, the gas-particle relative velocity is not changing when the bed is in fluidizing state. Therefore, the gas holdup plays an influential role in the reduction of the time and spatially averaged Nusselt numbers. By increasing the superficial gas velocity beyond the minimum fluidization velocity, the bed voidage increases, leading to a lower average Nusselt number calculated according to the Gunn correlation. Upon coarse-graining, the obtained Nusselt numbers are slightly reduced with
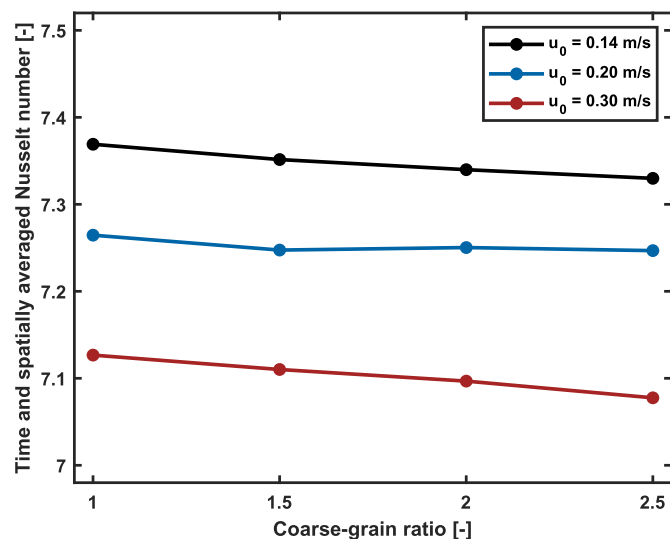
**Fig. 11.** Time and spatially averaged Nusselt number for the three different superficial velocities over coarse-graining ratio.

## 6. Conclusions

In this work, the CFD-DEM coarse-graining law of Sakai and Koshizuka (2009) is extended to gas-particle heat transfer. In coarse-graining fluidized bed simulations, the gas-particle heat transfer is dependent on the bed hydrodynamics. Therefore, the gas-particle two-way heat transfer was first verified via a packed bed test case. This test case showed that the coarse-graining scaling law perfectly coincides with the analytical solution. The fluidized bed heat transfer was studied using superficial gas velocities equal to 0.14, 0.20 and 0.30 m/s. Initially, hot solid material was placed in a 3D vertical column. By injecting a cold gas, the particle temperature decreases. The applied coarse-graining scaling law resulted in an excellent description of the original mean particle temperature. Small deviations between the particle temperature probability density functions and axial temperature profiles were found for the lowest superficial velocity case. Due to the averaging nature of coarse-graining, the bottom (cold) temperature region is not fully accurately describing the original system, resulting in small temperature PDF and axial profile deviations.

The gas-particle heat transfer was analyzed in terms of the Nusselt number. The Nusselt number, calculated from the Gunn correlation (Gunn, 1978), was accurately predicted by the coarse-graining scaling law. However, it was found that the time and spatially averaged Nusselt number slightly decreases with a maximum deviation equal to 1% compared to the original systems. Besides, the Nusselt number homogenizes upon coarse-graining due to the averaging nature of the applied scaling law.

This coarse-graining CFD-DEM gas-particle heat transfer extension reduces the computational load and allows one to accurately simulate heat transfer in larger gas-solid fluidized beds. An extension towards combined gas-solid heat and mass transfer will be evaluated in our future work.

**Declaration of competing interest**

The authors declare that they have no known competing financial interests or personal relationships that could have appeared to influence the work reported in this paper.

**Data availability**

A data package is available on doi:10.4121/8ba507a3-f0f6-49c8-a4ee-62700c20628f. Other data will be made available on request.

a maximum deviation equal to 1% compared to the original systems. Therefore, the coarse-graining scaling law is able to accurately predict the average Nusselt number of the original system.

The effect of coarse-graining on the distribution of the Nusselt number can be better described by probability density functions as shown in Fig. 12. Increasing the superficial gas velocity results in a wider Nusselt number distribution. This is directly correlated to the increased bubbling behavior and the decreasing emulsion phase fraction. Coarse-graining is able to describe these wider Nusselt number distributions upon increasing the superficial gas velocity. However, the coarse-graining averaging nature is also clearly observed in the obtained PDFs. As stated by Li et al. (2016) and highlighted in the discussion of Figs. 8, 9 and 10, high Nusselt number values are found in the bubble wakes while low values are observed in the bubble clouds respectively. Since the bubble wake and cloud regions are less pronounced, the corresponding effect is averaged out by the coarse-graining scaling law which is especially observed by the largest applied superficial gas velocity. On the other hand, for the lowest superficial gas velocity case, the bed is in a homogeneous state (as relatively small bubbles appear). Therefore, the effect of the coarse-graining averaging nature is less pronounced, resulting in smaller Nusselt number PDF differences.
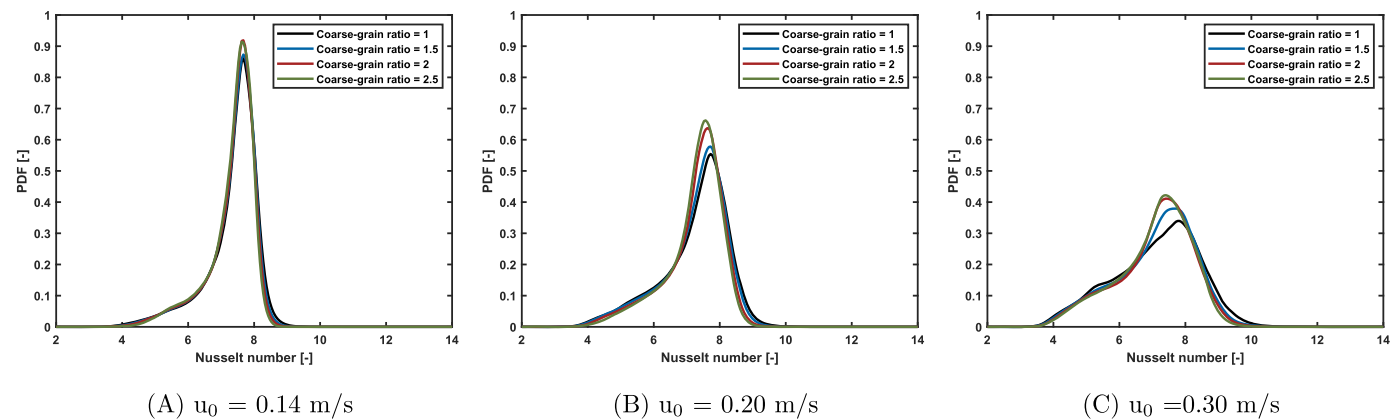


(A) $u_0 = 0.14$ m/s

(B) $u_0 = 0.20$ m/s

(C) $u_0 = 0.30$ m/s

**Fig. 12.** Normalized Nusselt number probability density functions for three different superficial velocities. Increasing the superficial gas velocity results in a wider distribution due to the increasing bubbling behavior. The coarse-graining scaling law is able to well predict the original system. Coarse-graining results in averaging of the original system and this effect is more pronounced for higher superficial gas velocities.

## Acknowledgements

## References

Aziz, H., Sansare, S., Duran, T., Gao, Y., Chaudhuri, B., 2022. On the applicability of the coarse grained coupled CFD-DEM model to predict the heat transfer during the fluidized bed drying of pharmaceutical granules. Pharm. Res. 39, 1991–2003.

Banaei, M., Jegers, J., Van Sint Annaland, M., Kuipers, J.A.M., Deen, N.G., 2017. Effect of superficial gas velocity on the solid temperature distribution in gas fluidized beds with heat production. Ind. Eng. Chem. Res. 56, 8729–8737.

Beetstra, R., van der Hoef, M.A., Kuipers, J.A.M., 2007. Drag force of intermediate Reynolds number flow past mono- and bidisperse arrays of spheres. AIChE J. 53, 489–501.

Benyahia, S., Galvin, J.E., 2010. Estimation of numerical errors related to some basic assumptions in discrete particle methods. Ind. Eng. Chem. Res. 49, 10588–10605.

Bird, R.B., Stewart, W.E., Lightfoot, E.N., 2007. Transport Phenomena. John Wiley and Sons, Inc.

Cundall, P.A., Strack, O.D.L., 1979. A discrete numerical model for granular assemblies. Geotechnique 29, 47–65.

de Munck, M.J.A., van Gelder, J.B., Peters, E.A.J.F., Kuipers, J.A.M., 2023. A detailed gas-solid fluidized bed comparison study on CFD-DEM coarse-graining techniques. Chem. Eng. Sci. 269, 118441.

Deen, N.G., van Sint Annaland, M., Kuipers, J.A.M., 2004. Multi-scale modeling of dispersed gas-liquid two-phase flow. Chem. Eng. Sci. 59, 1853–1861.

Deen, N.G., Van Sint Annaland, M., Van der Hoef, M.A., Kuipers, J.A.M., 2007. Review of discrete particle modeling of fluidized beds. Chem. Eng. Sci. 62, 28–44.

Di Renzo, A., Napolitano, E.S., Di Maio, F.P., 2021. Coarse-grain DEM modelling in fluidized bed simulation: a review. Processes 9, 1–30.

Du, S., Wang, J., Yu, Y., Zhou, Q., 2023. Coarse-grained CFD-DEM simulation of coal and biomass co-gasification process in a fluidized bed reactor: effects of particle size distribution and operating pressure. Renew. Energy 202, 483–498.

Golshan, S., Sotudeh-Gharebagh, R., Zarghami, R., Mostoufi, N., Blais, B., Kuipers, J.A.M., 2020. Review and implementation of CFD-DEM applied to chemical process systems. Chem. Eng. Sci. 221, 115646.

Gunn, D.J., 1978. Transfer of heat or mass to particles in fixed and fluidised beds. Int. J. Heat Mass Transf. 21, 467–476.

Hou, Q.F., Zhou, Z.Y., Yu, A.B., 2012. Computational study of the effects of material properties on heat transfer in gas fluidization. Ind. Eng. Chem. Res. 51, 11572–11586.

Kamath, S., Masterov, M.V., Padding, J.T., Buist, K.A., Baltussen, M.W., Kuipers, J.A.M., 2020. Parallelization of a stochastic Euler-Lagrange model applied to large scale dense bubbly flows. J. Comput. Phys. X 8, 100058.

Kuipers, J.A.M., van Duin, K.J., van Beckum, F.P.H., van Swaaij, W.P.M., 1993. Computer simulation of the hydrodynamics of a two-dimensional gas-fluidized bed. Comput. Chem. Eng. 17, 839–858.

Lau, Y.M., Bai, W., Deen, N.G., Kuipers, J.A.M., 2014. Numerical study of bubble break-up in bubbly flows using a deterministic Euler-Lagrange framework. Chem. Eng. Sci. 108, 9–22.

Li, Z., van Sint Annaland, M., Kuipers, J.A.M., Deen, N.G., 2016. Effect of superficial gas velocity on the particle temperature distribution in a fluidized bed with heat production. Chem. Eng. Sci. 140, 279–290.

Li, Z., van Sint Annaland, M., Kuipers, J.A.M., Deen, N.G., 2017. Effect of operating pressure on particle temperature distribution in a fluidized bed with heat production. Chem. Eng. Sci. 169, 299–309.

Liu, X., Deen, N.G., Tang, Y., 2021. On the treatment of bed-to-wall heat transfer in CFD-DEM simulations of gas-fluidized beds. Chem. Eng. Sci. 236.

Lu, L., Morris, A., Li, T., Benyahia, S., 2017. Extension of a coarse grained particle method to simulate heat transfer in fluidized beds. Int. J. Heat Mass Transf. 111, 723–735.

Madlmeir, S., Radl, S., 2022. A coarse-grained parcel method for heat and mass transfer simulations of spray coating processes. Adv. Powder Technol. 33, 103590.

Mori, Y., Wu, C.Y., Sakai, M., 2019. Validation study on a scaling law model of the DEM in industrial gas-solid flows. Powder Technol. 343, 101–112.

Mu, L., Buist, K.A., Kuipers, J.A.M., Deen, N.G., 2020a. Hydrodynamic and heat transfer study of a fluidized bed by discrete particle simulations. Processes 8, 1–15.

Mu, L., Buist, K.A., Kuipers, J.A.M., Deen, N.G., 2020b. Scaling method of CFD-DEM simulations for gas-solid flows in risers. Chem. Eng. Sci. X 6.

Patil, A.V., Peters, E.A.J.F., Kolkman, T., Kuipers, J.A.M., 2014. Modeling bubble heat transfer in gas-solid fluidized beds using DEM. Chem. Eng. Sci. 105, 121–131.

Patil, A.V., Peters, E.A.J.F., Kuipers, J.A.M., 2015a. Comparison of CFD-DEM heat transfer simulations with infrared/visual measurements. Chem. Eng. J. 277, 388–401.

Patil, A.V., Peters, E.A.J.F., Lau, Y.M., Kuipers, J.A.M., 2015b. Modeling 3D bubble heat transfer in gas-solid fluidized beds using the CFD-DEM. Ind. Eng. Chem. Res. 54, 11466–11474.

Radl, S., Radeke, C., Khinast, J.G., Sundaresan, S., 2011. Parcel-based approach for the simulation of gas-particle flows. In: 8th International Conference on CFD in Oil & Gas, Metallurgical and Process Industries, pp. 1–10.

Sakai, M., Koshizuka, S., 2009. Large-scale discrete element modeling in pneumatic conveying. Chem. Eng. Sci. 64, 533–539.

Sakai, M., Yamada, Y., Shigeto, Y., Shibata, K., Kawasaki, V.M., Koshizuka, S., 2010. Large-scale discrete element modeling in a fluidized bed. Int. J. Numer. Methods Fluids 64, 1319–1335.

Sakai, M., Abe, M., Shigeto, Y., Mizutani, S., Takahashi, H., Viré, A., Percival, J.R., Xiang, J., Pain, C.C., 2014. Verification and validation of a coarse grain model of the DEM in a bubbling fluidized bed. Chem. Eng. J. 244, 33–43.

Sutkar, V.S., Deen, N.G., Mohan, B., Salikov, V., Antonyuk, S., Heinrich, S., Kuipers, J.A.M., 2013. Numerical investigations of a pseudo-2D spout fluidized bed with draft plates using a scaled discrete particle model. Chem. Eng. Sci. 104, 790–807.

Syamlal, M., Gidaspow, D., 1985. Hydrodynamics of fluidization: prediction of wall to bed heat transfer coefficients. AIChE J. 31, 127–135.

Takabatake, K., Mori, Y., Khinast, J.G., Sakai, M., 2018. Numerical investigation of a coarse-grain discrete element method in solid mixing in a spouted bed. Chem. Eng. J. 346, 416–426.

Verma, V., Deen, N.G., Padding, J.T., Kuipers, J.A.M., 2013. Two-fluid modeling of three-dimensional cylindrical gas-solid fluidized beds using the kinetic theory of granular flow. Chem. Eng. Sci. 102, 227–245.

Wahyudi, H., Chu, K., Yu, A., 2016. 3D particle-scale modeling of gas-solids flow and heat transfer in fluidized beds with an immersed tube. Int. J. Heat Mass Transf. 97, 521–537.

Wang, S., Shen, Y., 2022. Coarse-grained CFD-DEM modelling of dense gas-solid reacting flow. Int. J. Heat Mass Transf. 184, 122302.

Wang, S., Luo, K., Hu, C., Fan, J., 2018. Particle-scale investigation of heat transfer and erosion characteristics in a three-dimensional circulating fluidized bed. Ind. Eng. Chem. Res. 57, 6774–6789.

Weinhart, T., Orefice, L., Post, M., van Schrojenstein Lantman, M.P., Denissen, I.F., Tunuguntla, D.R., Tsang, J.M., Cheng, H., Shaheen, M.Y., Shi, H., Rapino, P., Grannonio, E., Losacco, N., Barbosa, J., Jing, L., Alvarez Naranjo, J.E., Roy, S., den Otter, W.K., Thornton, A.R., 2020. Fast, flexible particle simulations — an introduction to MercuryDPM. Comput. Phys. Commun. 249, 107129.

Zhang, K., Wang, S., Li, B., He, Y., Zhao, Y., 2020. Heat transfer in a pulsed fluidized bed by using coupled CFD-DEM method. Powder Technol., 497–505.

Zhou, Z.Y., Yu, A.B., Zulli, P., 2009. Particle scale study of heat transfer in packed and bubbling fluidized beds. AIChE J. 55, 868–884.